WPMAT-PR(17) 17276

N Ordas et al.

XPS surface analysis of gas atomized powder precursor of ODS ferritic steels obtained through the STARS route

Preprint of Paper to be submitted for publication in
Applied Surface Science

This work has been carried out within the framework of the EUROfusion Consortium and has received funding from the Euratom research and training programme 2014-2018 under grant agreement No 633053. The views and opinions expressed herein do not necessarily reflect those of the European Commission.

XPS surface analysis of gas atomized powder precursor of ODS ferritic steels obtained through the STARS route

E. Gil, J. Cortés, I. Iturriza, N. Ordás

Ceit-IK4, 20018 San Sebastian, Spain

Abstract

Oxide Dispersion Strengthened Ferritic Stainless Steels (ODS FS) show high strength and creep resistance at elevated temperatures and good resistance to neutron radiation damage due to the presence of a high density of very stable nanometric oxides, generally rich in yttrium and titanium. Such behavior enables their use as high-temperature structural materials.

An innovative powder metallurgy route to produce ODS FS has succeeded in atomizing steel powders containing the oxide formers (Y and Ti) and, hence, avoids the mechanical alloying step to dissolve Y in the matrix. A metastable oxide layer forms at the surface of atomized powders, which dissociates during HIP consolidation at high temperatures and leads to precipitation of more stable Y-Ti-O nanoparticles.

Present work describes the oxide layer developed on spherical gas atomized powders with composition Fe-14Cr-2W-0.3Ti-0.18Y during the thermal treatment performed on powders to adjust the oxygen concentration before their consolidation. Scanning electron microscopy (SEM) combined with X-ray photoelectron spectroscopy (XPS) are used to analyze the composition and morphology of the oxide layer. Results demonstrate that it consists of a continuous 19-thick metastable Fe_2O_3 oxide layer, combined with discrete Cr_2O_3 and Y_2O_3 oxides grown preferentially at grain boundaries of the surface of powder particles.

1. Introduction

Oxide Dispersion Strengthened Ferritic Stainless Steels (ODS-FS) are promising materials for structural components in concentrated solar power plants, chemical reactors or advanced coal fired plants due to their creep resistance, high strength at elevated temperatures and low DBTT (Ductile-Brittle Transition Temperature) [1], [2], [3], [4], [5]. In addition, their good resistance to neutron irradiation damage make them exceptional candidate materials in future fission and fusion reactors [2], [6], [7]. Their outstanding behavior is a direct consequence of their very fine grain size, and the presence of extremely fine nanometric (3-4 nm) particles, generally yttrium and titanium complex oxides, with high temperature stability. These oxides have a pinning effect on dislocations and are sinks for irradiation induced defects [8], [9].

ODS-FS for fusion application are mainly produced with a composition in the range Fe-(12-14)Cr-(1-2)W-(0.25-0.5)Ti-(0.2-0.3) Y_2O_3 (wt.%) [7], [10], [11], [12], [13], [14], [15], [16], [17]. Chromium contents higher than 13 wt.% stabilizes alpha phase. Tungsten acts as solid solution strengthening whereas yttrium and titanium form strengthening Y-Ti-O precipitates with high temperature stability. Besides, titanium refines the precipitate dispersion in the matrix, which improves creep properties [5], [6].

ODS FS are produced by Powder Metallurgy (PM). The standard route starts with mechanical alloying (MA) of the elemental or gas atomized prealloyed Fe-Cr-W-Ti powders, with yttria particles to dissolve the yttrium in the ferritic matrix. The mechanically alloyed powders are encapsulated and consolidated at high temperature by Hot Isostatic Pressing (HIP) or hot extrusion to obtain a dense material and promote the precipitation of the oxide nanoparticles. Manufacturing of ODS FS includes final thermomechanical treatments (hot rolling), to promote recrystallization. [4], [13], [14], [15]. However, MA involves several drawbacks such as high time and cost inefficiencies, contamination from the grinding media, jars or atmosphere, difficulties in controlling the homogeneity of the alloy and presence of batch to batch heterogeneities.

With the aim of avoiding this step, a new processing route named STARS (Surface Treatments of gas Atomized powder followed by Reactive Synthesis), has been developed [18], [19]. This route is inspired in the GARS method (Gas Atomization Reactive Synthesis) developed by Rieken and Anderson [20], [21], [22]. The GARS method is based on the atomization of powder with a reactive gas (Ar-O_2) to form metastable chromium oxides on the surface of powder particles during their rapid cooling down. During the subsequent consolidation by HIP these oxides are dissociated, its oxygen becomes available to diffuse inside ferritic grains and reacts with the titanium and yttrium dissolved in the ferritic matrix or forming yttrium-rich intermetallic compounds. As a result, the strengthening Y-Ti-O nano-oxides precipitate in the ferritic matrix [8]. In the STARS route, the powder is atomized using inert gas, so its oxygen concentration is lower than the required values to obtain the Y-Ti-O nanoparticles. Therefore, the atomized powders have to undergo a thermal treatment at mild temperatures to adjust the oxygen content and form the metastable oxide layer on the surface of the particles. The oxide metastable layer of powders obtained with the STARS route, having been developed under conditions (temperature, time) different than those of powders of the GARS route, may consist of oxides of different nature than those identified in the GARS route. An unambiguous identification of oxides formed during the atomization and the surface treatment of powders is crucial in order to understand the oxygen exchange mechanisms leading to the precipitation of Y-Ti-O nano-oxides.

The objective of this work is to demonstrate that the oxides developed on the surface of as-atomized and thermal treated powders during the STARS route are metastable and, thus, can be dissociated during HIPping at high temperatures.

2. Materials and experimental procedure

Powders containing Y and Ti were produced by close-coupled gas atomization with argon at Ceit-IK4. The chemical composition of the atomized powder, measured by ICP (Inductively Coupled Plasma), and the concentration of interstitials obtained with the inert gas fusion principle (N, O) and combustion infrared detection technique (C, S) are shown in Table 1:

Table 1. Composition of powders (wt.%).

Element	Fe	Cr	W	Ti	Y	Al	O	C	N	S
Concentratio	Bal	14,2	2,00	0,30	0,18	0,00	0,02	0,0,	0,00	0,00

n	.					8	5	9	1	2

Atomized powders with a size fraction of 20-45 µm in diameter were heat treated under oxidizing atmosphere at low temperatures (below 350 °C) to ensure logarithmic oxidation kinetics.

Chemical analysis of the surface of powder particles was performed by X-ray Photoelectron Spectroscopy (XPS) using a monochromatic source of X-ray Al Kα (1486.6 eV). The elemental composition and the oxidation state of the elements present in the atomized powder were obtained. All binding energies of different XPS spectra were referenced to C1s peak of 284.9 eV, to provide accurate energy calibration, and a surface of 750 x 250 μm^2 was always analyzed to provide a reliable and representative average composition of the zone of interest. For simplicity, no corrections for the spherical shape of the powder were introduced. Determination of the oxide layer thickness and the evolution in depth of its chemical composition was done by combining successive XPS analysis with argon ion beam etching. The total thickness of the layer analyzed is about 60 nm.

The microstructure at the surface of powder particles was examined before and after heat treatment with a FEG-SEM (Field Emission Gun - Scanning Electron Microscope) equipped with EDS (Energy Dispersive Spectroscopy) analyzer. The results were correlated with XPS findings.

3. Results and discussion

3.1. XPS analysis

Figure 1 shows the spectra corresponding to XPS analysis performed on the surface of as-atomized and oxidized powder particles. As can be seen, titanium and tungsten peaks are hardly resolvable and, consequently, were not taking into account in the analysis. The intense carbon peaks (C1s) correspond to adsorbed organic species on the surface of powder particles and, as it is shown below, is strongly decreased after ion etching. Therefore, this element has not been taken into account in this study. The increase in the intensity of the oxygen peak (O1s) after oxidation is consistent with the increase in the oxygen concentration (from 0.02 wt. % in as-atomized powder to 0.07 wt.% after oxidation). Also the intensity of the iron peak (Fe2p) raises after oxidation, while the yttrium peaks are weaker, especially the Y3d peak.

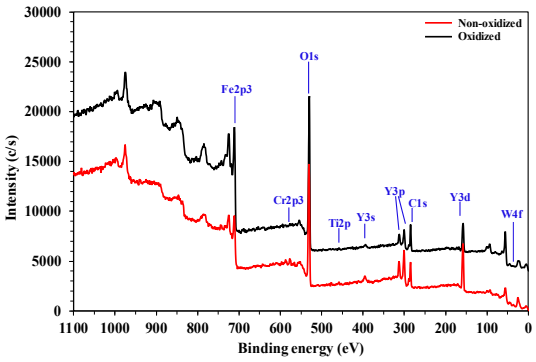

Figure 1. XPS survey spectra of as-atomized powder and oxidized powder.

The fact that the yttrium peaks are clearly resolvable in Figure 1, despite its low concentration (0.34 wt.%), indicates yttrium enrichment at the surface of both as-atomized and oxidized powder particles. Titanium and tungsten peaks are hardly resolvable, their presence is just above the threshold detection of low resolution XPS analysis and, therefore, they can be neglected during further calculations.

Figure 2 and Figure 3 show the XPS depth profile analyses of the as-atomized and oxidized powder particles, up to about 60 nm. Carbon signal, associated to adsorbed C-rich species and restricted to 2 nm was removed and was not considered in this work. Depth profile analyses also confirm the local enrichment of yttrium at the very surface of the powder particles, independently of whether they have been oxidized. During atomization, and as soon as the melt droplets are exposed to the inert gas atomization containing a residual concentration of oxygen, yttrium diffuses towards the surface and immediately oxidizes. After comparing O and Fe curves from Figure 2 left and Figure 2 right, it is straightforward that the concentration of iron and oxygen increased after oxidation, due to iron oxidation, which leads to a relative depletion of chromium and yttrium at the surface. In addition, titanium and tungsten only appear at 40 nm etch depth, suggesting that these elements do not diffuse towards to the surface neither during solidification and cooling down of atomized powder particles nor during oxidation at low temperature, as expected.

XPS depth profile analyses disregarding the contribution of interstitial elements are shown in Figure 3. The most significant changes in concentration associated to the oxidation of powder correspond to iron, chromium and yttrium elements, from largest to smallest. After oxidation, the concentration of iron at the surface (0 nm) increases from 45 at.% to 79.5 at.%. However, the presence of chromium and yttrium at the surface and down to 20 nm depth is reduced after oxidation. From this depth the oxidation of powders do not apparently alter the concentration of these two elements, which suggests that the thickness of the superficial oxide layer after oxidation is in the order of 20 nm. Accurate calculation of the thickness of the oxide layer thickness is accurately determined later by high resolution XPS spectra.

An increase in the iron concentration at the surface after oxidation suggests that this element oxidizes preferentially, in comparison to the other alloying elements. Therefore, and in agreement with other studies [23], [24], [25], the main component of the oxide scale developed at the surface during the heat treatment of powder particles is iron. Nyborg demonstrated that during the gas atomization of a ferritic powder with 25 wt. % of chromium, a 3 nm-thick continuous iron oxide layer is instantly developed as soon as melt drops are exposed to the atomization gas [9]. Since, in practice, is not possible to ensure an oxygen concentration of 0 ppm during gas atomization, this iron oxide layer is inherent to gas atomized steel powders. Additionally, ultrafine nanometric oxide particles rich in the strong oxide forming alloying elements (chromium, titanium and yttrium) are expected to be present at the surface of atomized powder particles, together with the very thin iron oxide layer

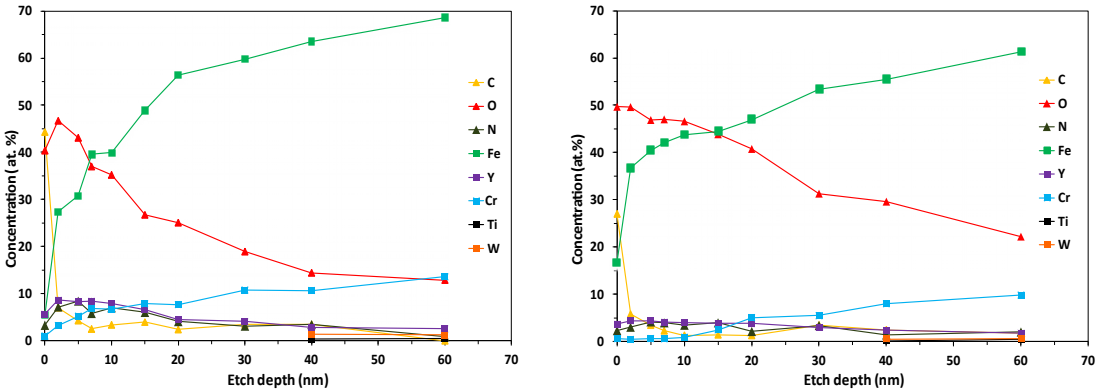

Figure 2. Depth profile analysis of the elements concentration obtained by XPS analysis at low resolution before (left) and after powder oxidation (right).

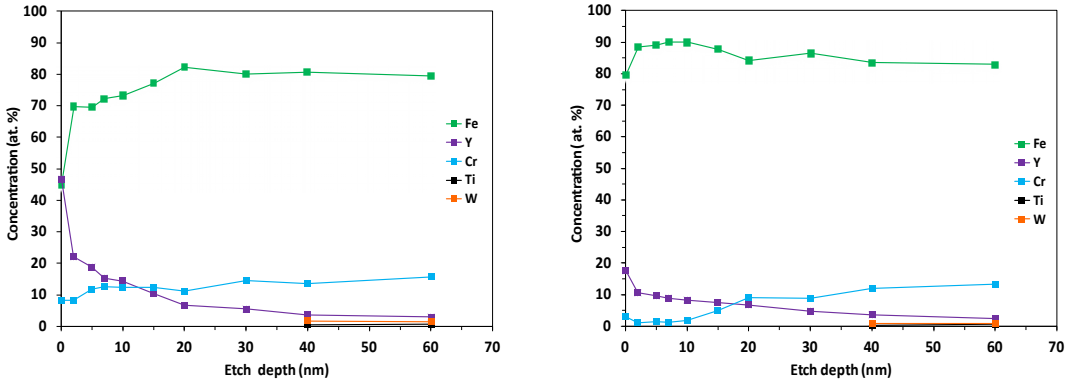

Figure 3. Depth profile analysis of the elements concentration obtained by XPS analysis at low resolution before (left) and after powder oxidation (right), removing contribution of interstitials.

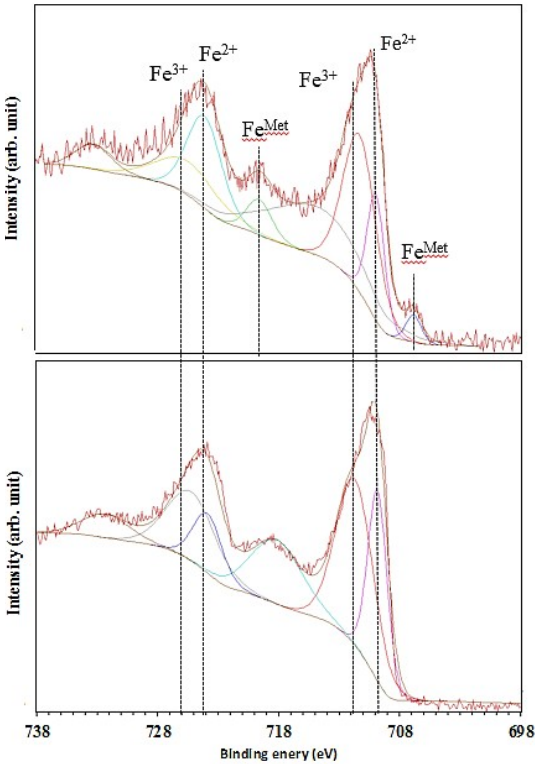

Figure 4. Detailed XPS spectra of iron at the surface of as-atomized (top) and oxidized powder (bottom).

Detailed high-resolution spectra of Fe, Y, Cr and O, which provide information about chemical state of the elements, are shown in Figure 4 and Figure 5.

The Fe 2p doublet spectra at the surface of as-atomized and oxidized powder are shown in Figure 4 and indicate that after atomization only a small fraction of iron remains metallic, being the oxide layer composed by both Fe_2O_3 (Fe^{3+}) and FeO (Fe^{2+}) Fe^{2+}. After heat treatment, the surface of powder particles is completely oxidized. The relative composition of the oxide at the surface has been estimated from the areas of Fe^{2+} and Fe^{3+}peaks, and it has been found that it is mainly composed by Fe_2O_3 (about 95 wt.%), regardless of whether the powder has been oxidized or not. With increasing etching depth (Figure 5), the relative intensity of Fe^0 metallic iron peaks increases at the expense of iron oxide peak, and Fe^0 metallic peak appears at 10 nm depth. After etching to 20 nm, the Fe^{3+} (Fe_2O_3) and Fe^{2+} (FeO) contribution to the Fe 2p spectrum is almost negligible. It can be concluded that the iron oxide has a thickness lower than 10 nm and iron is mainly metallic at depths above 20 nm in the as atomized powder. After surface oxidation of powder particles, Fe^0 metallic peak is only resolvable at depths above 20 nm (Figure 5b), and only after etching down to 50 nm iron is mainly metallic, as the presence of the prominent Fe^0 peak at about 706,5 eV in Figure 5b indicates. This evidences that iron oxide layer has grown during oxidation. Full removal of intensive iron oxide signal (Fe^{3+} and Fe^{2+}) with etching depth indicates that iron oxide is only present as a surface layer.

Chromium is also present as oxide at the surface of as-atomized powders, as the Cr 2p spectra in Figure 5c show (Cr^{3+} cation, $2p_{3/2}$ and $2p_{1/2}$ peak positions at 576 and 586 eV, respectively). Again, the contribution of chromium metallic peak, at about 574 eV [26], which appears after etching to 10 nm, increases with increasing etching depth, and is mainly metallic chromium at

50 nm from the surface. After oxidation of powder, chromium remains completely oxidized down to 20 nm, and even at 50 nm from the surface the corresponding oxide peaks can be clearly distinguished (Figure 5d). The higher intensity of chromium oxide peaks at intermediate depths (20-50 nm) in the oxidized powder indicates that this oxide has an inhomogeneous thickness. The presence of chromium oxides after almost complete removal of iron oxide in oxidized powders (compare Figure 5b and Figure 5d) suggests that chromium forms 'oxide islands' on the surface of powder particles, as proposed by [28].

The peak pairs with binding energies about 156,8 eV and 158,8 eV observed in Figure 5e correspond to Y $3d_{5/2}$ and Y $3d_{3/2}$ [29] and indicate that yttrium is almost completely oxidized in the as-atomized powder, regardless of the analyzed depth. The reduction of their intensity with increasing depth suggests yttrium segregation at the surface of powder particles during the atomization process. Only at depths above 20 nm the slight broadening of the peak at lower binding energy may suggest the presence of metallic yttrium, whose peak is located at a binding energy of 156,0 eV [30]. After oxidation, the detailed scan for Y 3d peak (Figure 5f) clearly shows that yttrium is completely oxidized. Only the broadness of the data collected at the highest depth (50 nm) suggests that yttrium may be partially metallic. The broad peak at 2 nm can be explained considering the hygroscopic nature of yttrium oxide through the presence of the Y-OH peak at about 157,5 eV [30]. The maximum concentration of yttria is located at intermediate depths, at 10-20 nm from the surface, suggesting yttrium is also forming discontinuous 'oxide islands' at the surface of powder particles.

The broadened shape of the oxygen O 1s spectrum of the surface (0 nm) in Figure 5f and h suggests that the oxygen is present in at least two states, and the contribution of metallic oxides (O^{2-}) and hydroxyl group (OH^-) can be distinguished. The OH^- group, related to hydroxides formed after superficial adsorption of environmental humidity, is removed after slight etching. After oxidation, the intensity of metallic oxide peaks increases, as expected.

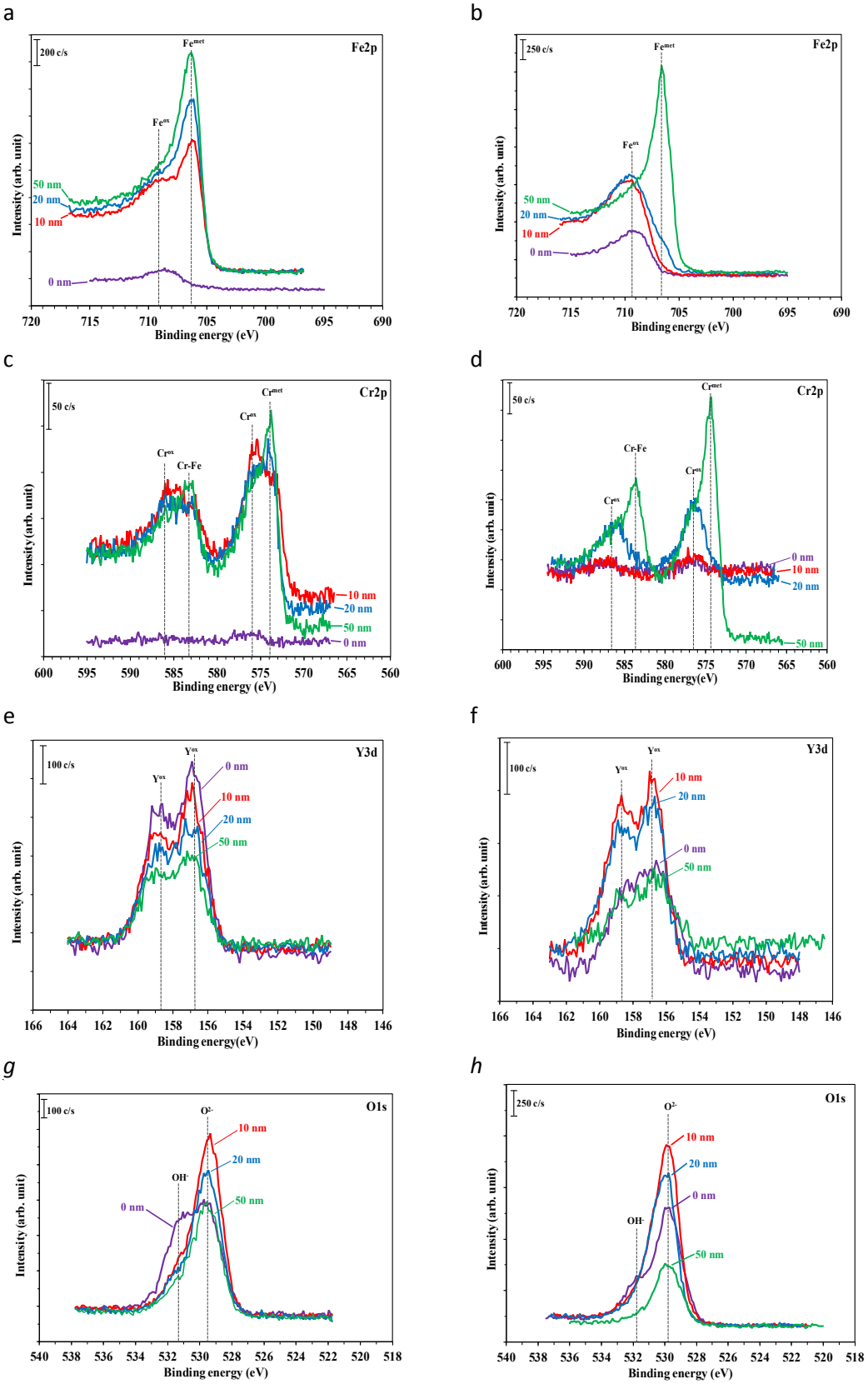

Figure 5. Detailed XPS spectra of iron, yttrium, chromium and oxygen of as-atomized (left) and oxidized powder (right) at the surface (0 nm depth) and 10, 20 and 50 nm from the surface.

3.2. Estimation of oxide layer thickness

The analysis of high resolution narrow XPS scans indicate that surface chromium oxidation into Cr_2O_3 and yttrium segregation and oxidation into Y_2O_3 occurs during cooling of gas atomized powder, while the particles are still at high temperatures, due to the high affinity of Y and Cr for oxygen and its elevated oxidation kinetics [31]. However, iron is oxidized at lower temperatures, when powder is manipulated and exposed to air atmosphere as it is shown in [10]. Consequently, Cr_2O_3 and Y_2O_3 oxides develop at the surface of powder particles as isolated particles whereas iron oxides (mainly Fe_2O_3, plus minority FeO) form a continuous superficial layer between these oxide particles.

The thickness of this continuous surface iron oxide layer can be estimated from the evolution with depth of the intensity of the Fe^0 iron metallic peak normalized to its intensity in the bulk, where iron is fully metallic. Assuming this oxide layer consists of Fe_2O_3, the iron metallic relative intensity at the transition oxide/metal is 65-70 % [27], [28], [32]. An alternative method estimates the thickness of the oxide layer as the etch depth whose peak relative intensity corresponds to the average value of the minimum and maximum relative intensities of the oxygen peak [24], [28], [32]. The Fe_2O_3 oxide thickness obtained with both methods is very similar, about 7.5 nm in the as-atomized powder and about 19 nm after oxidation (Figure 6).

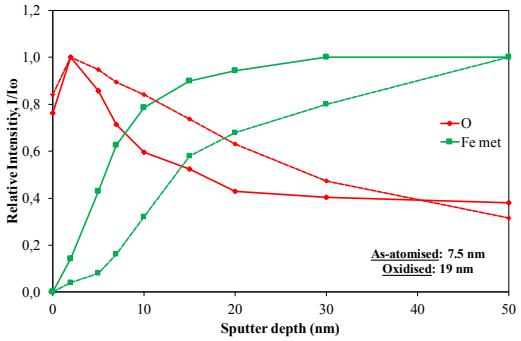

Figure 6. Estimation the thickness of the iron oxide layer by normalized intensity of metallic Fe and oxygen peak for (left) as-atomized powder and (b) oxidized powder.

The thickness of the oxide layer can be also estimated with the chemical granular analysis [33], from the plot oxygen concentration-specific surface area (or inverse of diameter of powder particle, D, see Figure 7). Assuming spherical particles covered with a continuous and homogeneous surface-oxide layer mainly composed by of Fe_2O_2 and Cr_2O_3, the chemical-granular approach estimates a thickness of the oxide layer that ranges from 16 to 18 nm before oxidation, and 57 to 59 nm after oxidation. The reason for discrepancies with the thickness obtained from XPS analysis is possibly due to the roughness of the surface and the presence of powder particles with irregular shape and satellites, which consequently underestimate the specific surface of the powder particles. Measurement of surface area by BET would provide more accurate oxide thickness values from the oxygen concentration.

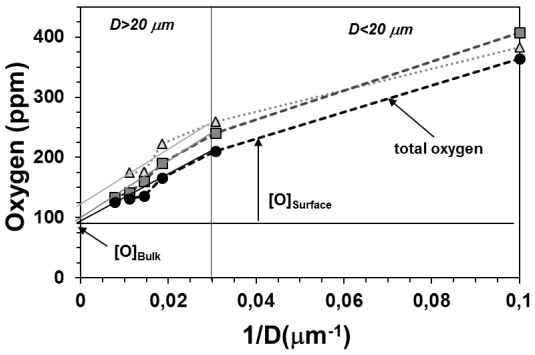

Figure 7. Oxygen concentration as a function of the inverse of diameter of powder particles

1.1. SEM + EDS analysis

As-atomized powder

The surface of as-atomized and heat-treated steel powders was observed by FEG-SEM in order to determine the size and distribution of the oxides identified by XPS. The depth analyzed by EDS is larger than that of XPS and provides information of depths up to 100 nm in this work (5 kV).

As-atomized powders are mainly spherical (Figure 8a), although some of them contain satellites and splat caps caused by collisions between particles during solidification. At high magnification the surface of the spherical as-atomized powder particles is smooth (Figure 8b), with a random distribution of nanometric particles, preferentially at grain boundaries. Necks connecting particles with satellites show profuse precipitation at grain boundaries.

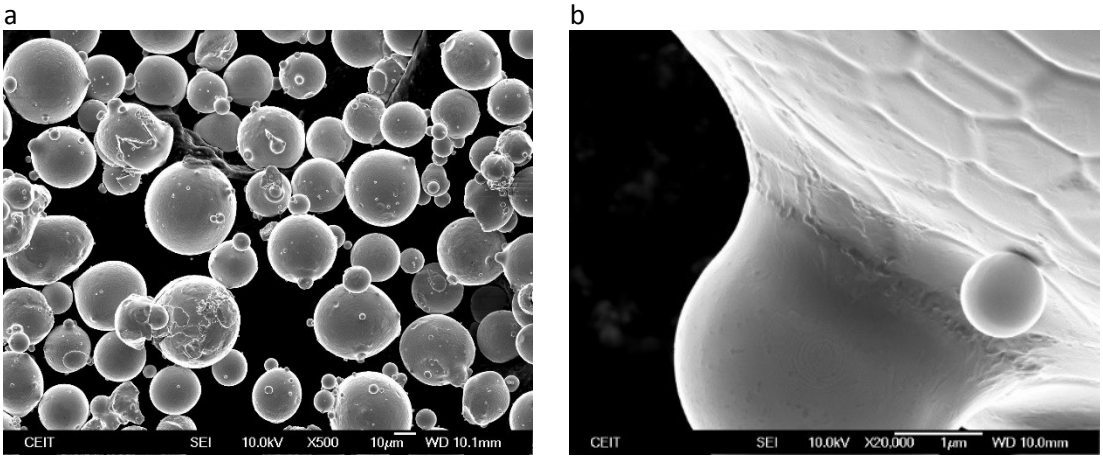

Figure 8. SEM image of the surface of as-atomized powder.

Cr_2O_3 particles could not detected at the surface of powder particles by SEM. At high magnification it can be observed that yttrium is preferentially located at triple points of the surface of powder particles (Figure 9). Continuous Y-rich segregation and precipitation can be observed by EDS analysis at grain boundaries, especially of largest powder particles (Figure 10). The fact that the oxygen concentration remains almost steady across the grain boundary where these Y-rich features are observed, suggests yttrium is majority metallic. XAS (X-ray adsorption spectroscopy) confirmed the metallic nature of yttrium in the atomized powders

[34]. Thus, Y_2O_3 phase detected by XPS (Figure 5 e and f) to a depth of 50 nm corresponds to the outer layer of the Y-rich precipitates found at the surface of powder particles, whose size can reach 400 nm.

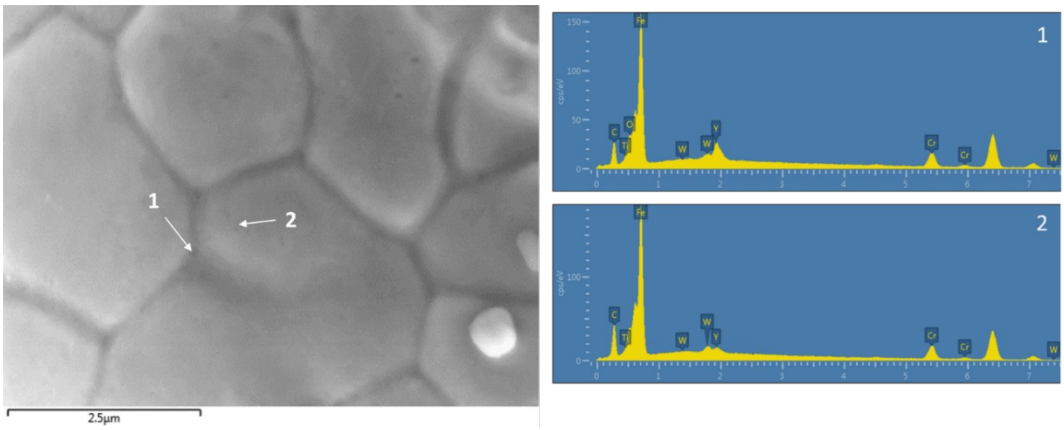

Figure 9. SEM image and EDS analysis of as-atomized powder showing Y segregation at triple points (particle size about 20 µm).

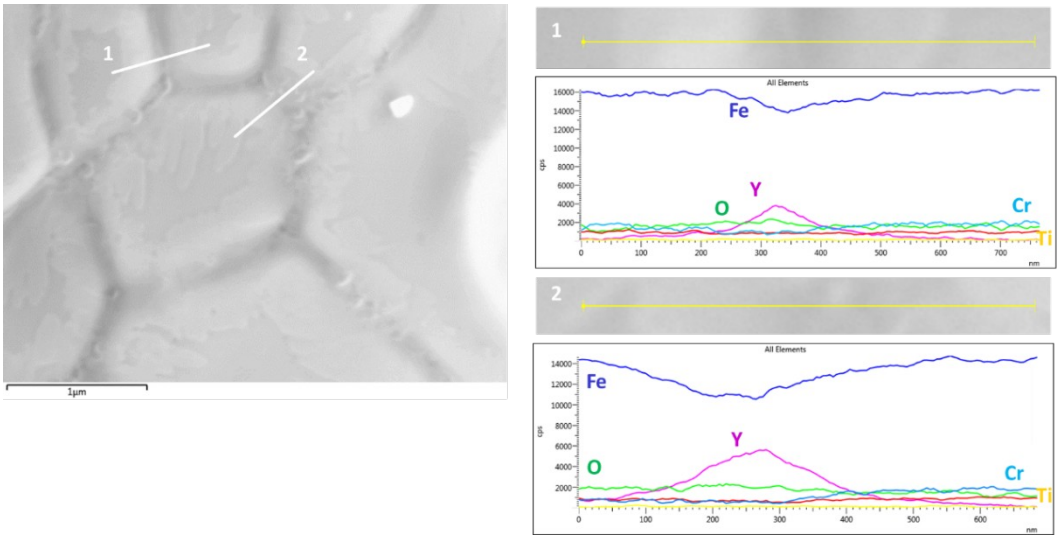

Figure 10. SEM image and EDS line analysis of as-atomized powder showing Y segregation and precipitation at grain boundaries (particle size about 20 µm).

As can be observed in Figure 11, there is a correlation between the morphology of Y-rich precipitation at the surface and the particle size of atomized powders. Yttrium remains in oversaturated solid solution in particles below 5 µm in diameter, and Y-rich segregates are not observed by SEM. Particles with size ranging from 5-45 µm contain a discrete distribution of intergranular Y-rich precipitates, whose size increases with powder particle size. Finally, this Y-rich phase evolves towards micrometric scale in largest particles, with high contiguity in powders above 75 µm. The morphological evolution of Y-rich features can be explained considering the extremely low solubility of yttrium in iron and steel (about 0.12 wt%. at 1320 °C, 0.05 wt% at 800 °C, and negligible at room temperature), and the relationship between particle size and its cooling rate during cooling down after solidification [36], [37]. When the atomized melt droplets solidify and cool down, Y oversaturated is rejected to highly disordered areas during nucleation and growth of the ferritic grains, resulting in Y microsegregation at grain boundaries. Whilst the cooling rate after solidification of the finest particles is extremely

high, even being able to prevent yttrium segregation and precipitation, the largest particles cool down much more slowly. This allows the oversaturated yttrium to diffuse towards more energetically favorable sites, like grain boundaries or free surfaces, and precipitate, as seen in Figure 11.

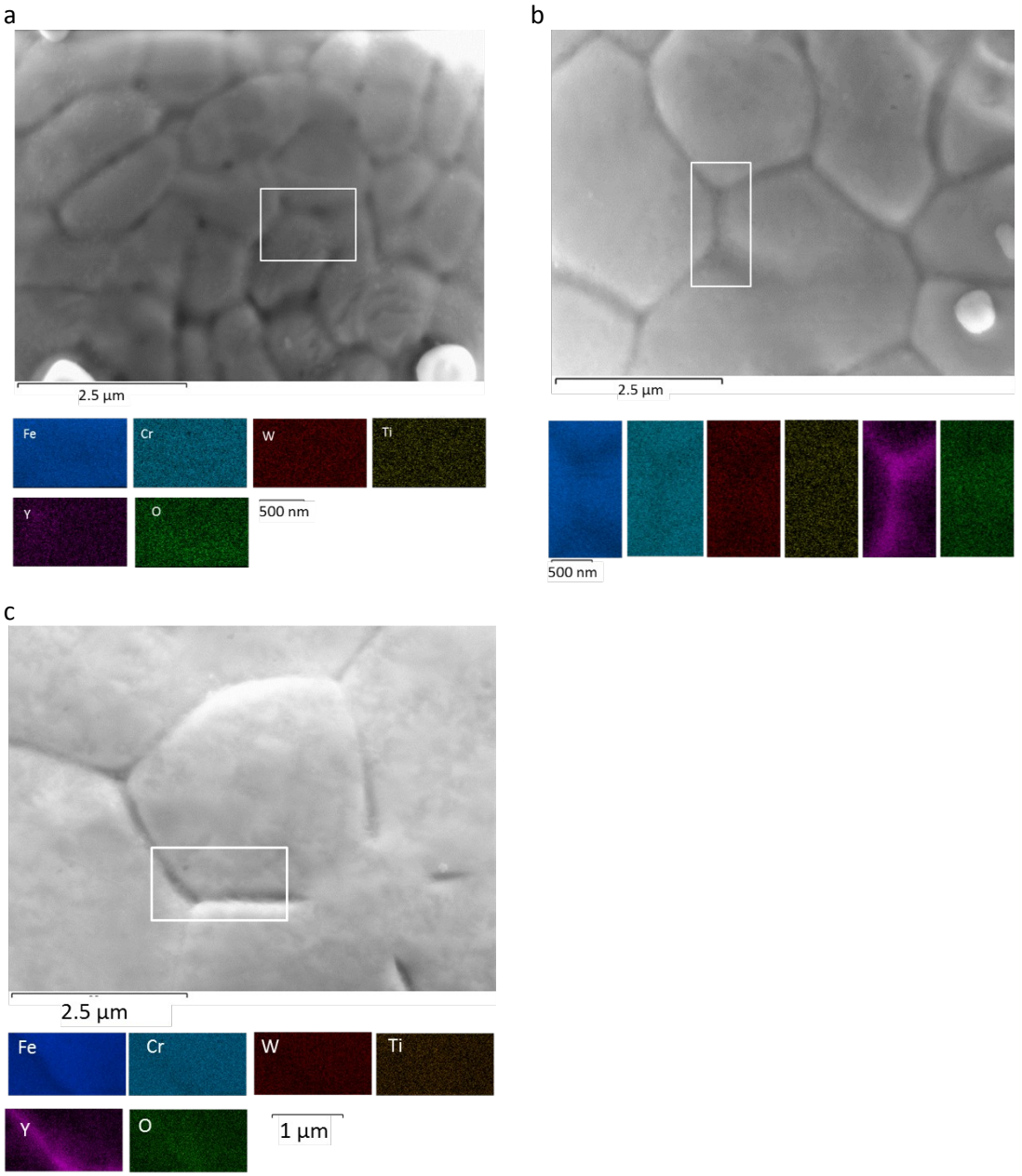

Figure 11. SEM images and EDS mapping analysis of as-atomized powder with different particle size ((a) <20 µm, (b) 20-45 µm and (c) 63-75 µm showing Y segregation and precipitation at grain boundaries.

1.1.1. Oxidized powder

Oxidation of powder resulted in an increase in the roughness of the surface of powder particles and the development of continuous chains preferentially located at grain boundaries and sub-grain boundaries as well as at the base of satellites attached to powder particles

(Figure 12a). During oxidation, discontinuous chains develop initially at grain boundaries of particle-satellite necks, with negative radius of curvature (concave). With increasing time or temperature, chains become continuous and thick, and grow at grain boundaries far from satellites. Observation at high magnifications reveals that these chains are in fact double (Figure 12b). Also thinner chains are observed inside grains, probably grown at subgrain boundaries.

EDS analyses of the oxidized surface, presented in Figure 13, evidences that this chains consist of a Y_2O_3 chain, grown on the grain boundary from the oxidation of Y-rich metallic particles, and flanked by two Cr_2O_3 chains, grown from oxidation of chromium-enriched areas at proximities of grain boundaries. Local chromium-enrichment in the proximities of grain boundaries can be attributed to the preferential diffusion of chromium along grain boundaries towards gas/oxide interface during oxidation at low temperatures [38]. These chains are in fact the "oxide islands" proposed from XPS analysis to have grown during the oxidation of powder. EDS analysis of the surface also shows a preferential diffusion of titanium towards grain boundaries. However, since titanium was not detected by XPS analyses, it is expected its diffusivity in this alloy is lower than that of chromium.

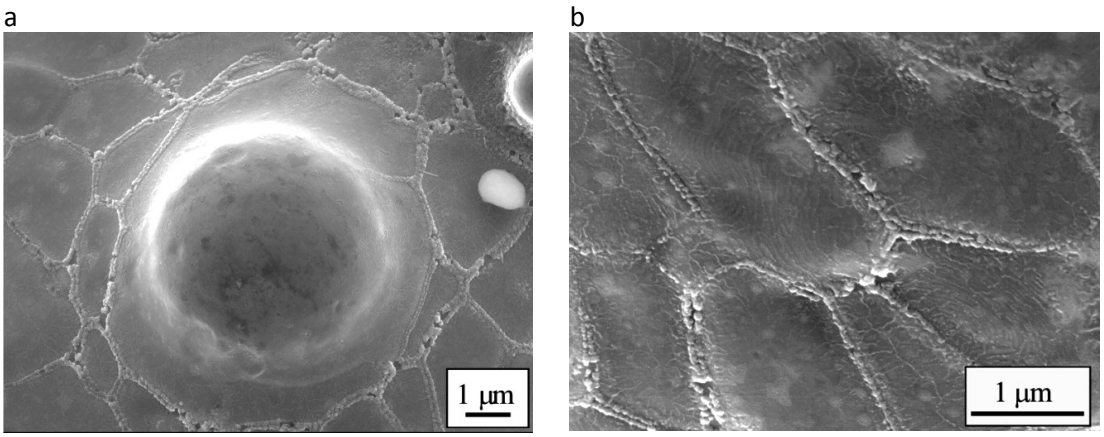

Figure 12. Morphology of powder after oxidation showing oxide chains mainly on grain boundaries.

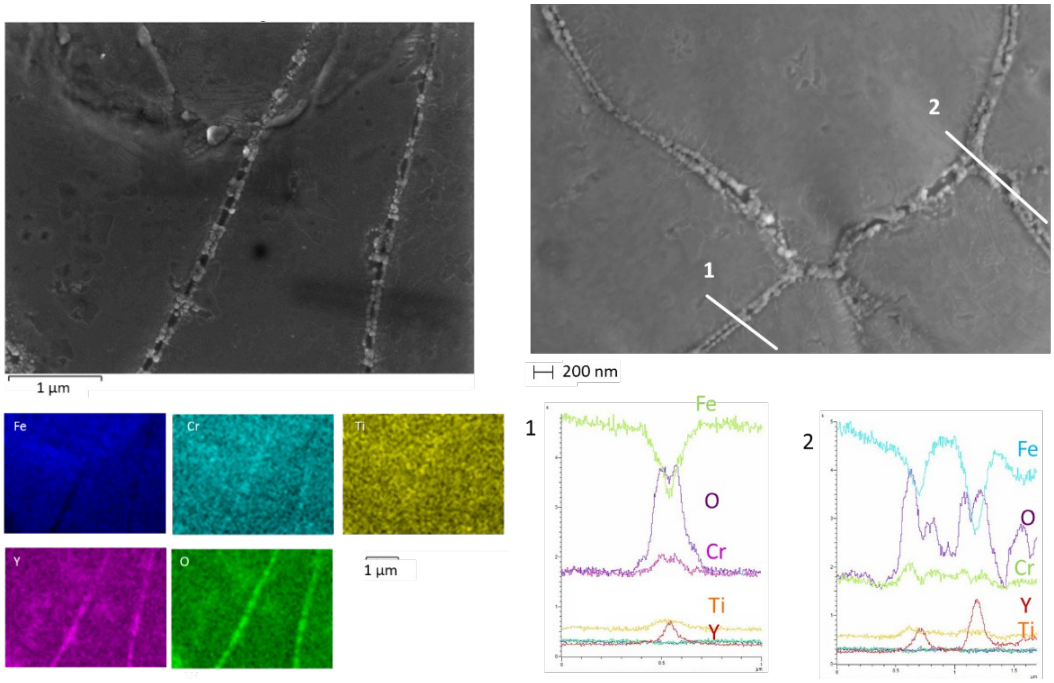

Figure 13. SEM images, EDS mapping and EDS linescan of oxidized powder.

2. Conclusions

This study has demonstrated that a metastable oxide thin layer is form at the surface of gas-atomized powders with composition Fe-14,2Cr-2W-0,3Ti-0,18Y during oxidation at temperatures below 350 °C. This oxide layer consists of an ultra thin Fe_2O_3 19 nm-thick continuous layer and oxide chains of Y_2O_3 flanked, in turn, by two Cr_2O_3, grown on grain and subgrain boundaries. These oxides are already present to a lesser extent in the as-atomized powders, and its thickness is estimated to be 7 nm.

Y_2O_3 develops from oxidation of submicrometric Y-rich metallic precipitates at grain boundaries of the surface of powder particles. Cr_2O_3 forms due to the chromium diffusion along grain boundaries towards the surface of powder particles exposed to oxygen.

The Fe_2O_3 and Cr_2O_3 metastable oxides will dissociate during consolidation of powder at high temperatures, and highly thermodynamically stable complex Y-Ti-O nanoparticles will form thanks to the oxygen exchange between these metastable oxides present at prior particle boundaries and the metallic ytrrium and titanium present in the ferritic matrix.

Acknowledgements

The authors would like to thank the foundation Institute of Nanoscience of Aragón (INA) for performing XPS analysis. This work has been carried out within the framework of the EUROfusion Consortium and has received funding from the Euratom research and training programme 2014-2018 under grant agreement No 633053. The views and opinions expressed herein do not necessarily reflect those of the European Commission.

References

[1] D. T. Hoelzer, J. Bentley, M. A. Sokolov, M. K. Miller, G. R. Odette, and M. J. Alinger, "Influence of particle dispersions on the high-temperature strength of ferritic alloys," *Journal of Nuclear Materials*, vol. 367–370, pp. 166–172, Aug. 2007.

[2] D. A. McClintock, D. T. Hoelzer, M. A. Sokolov, and R. K. Nanstad, "Mechanical properties of neutron irradiated nanostructured ferritic alloy 14YWT," *Journal of Nuclear Materials*, vol. 386–388, pp. 307–311, Apr. 2009.

[3] J. Hurley, "Applications for Dispersion-Strengthened Alloys in Thermal Power Systems," Proceedings of the Twenty Fisrt Annual Conference On Fossil Energy Materials, Knoxville, Tennessee, 2007.

[4] Z. Oksiuta et al., Mechanical properties and thermal stability of nanostructured ODS RAF steels, Mechanics of Material 67 (2013) 15-24.

[5] Z. Oksiuta et al., Microstructure examination of Fe-14Cr ODS ferritic steels produced through different processing routes. Journal of Nuclear Materials 451 (20014) 320-327

[6] D.A. McClintock et al., Mechanical properties of irradated ODS-EUROFER and nanocluster strengthened 14YWT, Journal of Nuclear Material 392 (2009), 353-359.

[7] N. Baluc, J. L. Boutard, S. L. Dudarev, M. Rieth, J. B. Correia, B. Fournier, J. Henry, F. Legendre, T. Leguey, M. Lewandowska, R. Lindau, E. Marquis, a. Muñoz, B. Radiguet, and Z. Oksiuta, "Review on the EFDA work programme on nano-structured ODS RAF steels," *Journal of Nuclear Materials*, vol. 417, no. 1–3, pp. 149–153, Oct. 2011.

[8] T. Chen et al., Microstructural changes and void swelling of a 12Cr ODS ferritic-martensitic alloy after high-dpa self-ion irradiation. Journal of Nuclear Materials 467 (2015), 42-49.

[9] M. Ratti, D. Leuvrey, M. H. Mathon, and Y. de Carlan, "Influence of titanium on nano-cluster (Y, Ti, O) stability in ODS ferritic materials," *Journal of Nuclear Materials*, vol. 386–388, pp. 540–543, Apr. 2009.

[10] Ch.Ch. Eiselt et al., Tensile and fracture toughness properties of the nanostructured oxide dispersion strengthened ferritic alloy 13Cr-1W-0.3Ti-0.3Y2O3. Journal of Nuclear Materials 417 (2011) 193-196.

[11] I. Hilger et al., Fabrication and characterization of oxide dispersion strengthened (ODS) 14Cr steels consolidated by means of hot isostatic pressing, hot extrusion and spark plasma sintering, Journal of Nuclear Materials 472 (2016) 206-214.

[12] J.H. Kim et al., Effects of processing condition on the microstructural and tensile properties of 14Cr-based oxide dispersion strengthened alloys. Journal of Nuclear Materials 449 (2014) pp 300-307.

[13] Z. Oksituta et al., Development and characterization of a new ODS ferritic steel for fusion reactor application. Journal of Nuclear Materials 393 (2009) 114-119.

[14] Z. Oksiuta et al., Influence of hot rolling and high speed hydrostatic extrusion on the microstructure and mechanical properties of an ODS RAF steel. Journal of Nuclear MAterials 409 (2011) 86-93.

[15] P. He et al., The influence of thermomechanical processing on the microstructure and mechanical properties of 13.5Cr ODS steels. Fusion Engineering and Design 88 (2013) 2448-2452

[16] P. He, M. Klimenkov, R. Lindau, and A. Möslang, "Characterization of precipitates in nano structured 14% Cr ODS alloys for fusion application," *Journal of Nuclear Materials*, vol. 428, no. 1–3, pp. 131–138, Sep. 2012.

[17] J. Hoffmann et al., Microstructural anisotropy of ferritic ODS alloys after different production routes. Fusion Engineering and Design 98-99 (2015) 1986-1990.

[18] E- Gil, N. Ordás, C. García-Rosales and I. Iturriza, Microstructural characterization of ODS ferritic steels at different processing stages, Fusion Engineering and Design 98-99 (2015)

1973-1977
[19]E. Gil, N. Ordás, C. García-Rosales and I. Iturriza, ODS ferritic steels produced by an alternative route (STARS): microstructural characterisation after atomisation, HIPping and heat treatments, Powder Metallurgy, 59:5 (2016), 359-369.
[20] J.R. Rieken, I. E. Anderson, and M.J. Kramer, Microstructure evolustion of gas-atomized iron-base ODS alloys, International Journal of Powder Matellurgy, 46, 6 (2010) 17-31.
[21]J. R. Rieken, I. E. Anderson, and M. J. Kramer, "Gas atomized chemical reservoir ods ferritic stainless steels," *Advances in Powder Metallurgy & Particulate Materials, MPIF, Hollywood, Fl, 2010*, pp. 112–131.
[22]J. R. Rieken, I. E. Anderson, M. J. Kramer, G. R. Odette, E. Stergar, and E. Haney, "Reactive gas atomization processing for Fe-based ODS alloys," *Journal of Nuclear Materials*, vol. 428, no. 1–3, pp. 65–75, Sep. 2012.
[23]I. Olefjord, "ESCA-studies of the composition profile of low temperature oxide formed on chromium steels - I. Oxydation in dry oxygen", Corrosion Science, Vol 15. (1975), pp. 687-696.
[24]L. Nyborg and E. Hryha, "Surface Oxides on Gas and Water Atomized Steel Powders," *Advances in Powder Metallurgy & Particulate Materials*, vol. 2, pp. 153–161, 2014.
[25]I. Olefjord and L. Nyborg, "Surface Analysis of Gas Atomized Ferritic Steel Powder," *Powder Metallurgy*, vol. 28, no. 4, pp. 237–243, Jan. 1985.
[26]M.C. Biesinger et al., X-ray photoelectron spectrospopy studies of chromium compounds, Surface and Interface Analysis 36 (2004), 1550-1563.
[27]D. Chasoglou, E. Hryha, M. Norell, and L. Nyborg, "Characterization of surface oxides on water-atomized steel powder by XPS/AES depth profiling and nano-scale lateral surface analysis," *Applied Surface Science*, vol. 268, pp. 496–506, Mar. 2013.
[28]E. Hryha, C. Gierl, L. Nyborg, H. Danninger, and E. Dudrova, "Surface composition of the steel powders pre-alloyed with manganese," *Applied Surface Science*, vol. 256, no. 12, pp. 3946–3961, Apr. 2010.
[29] S.A. Barve et al.,. Applied Surface Science 257 (2010) 215–221
[30]Mongstadetal./SolarEnergyMaterials&SolarCells128(2014)270–274
[31]S.B. Shendye, Role of yttrium in the high temperature oxidation of Ni-25wt%Cr alloys (1994), PhD Thesis, Oregon Graduate Institute of Science & Technology. Scholar Archive. Paper 3399.
[32]L. Nyborg, A. Nylund, and I. Olefjord, "Thickness Determination of oxide Layers on Spherically-shaped Metal Powders by ESCA," *Surface and Interface Analysis*, vol. 12, pp. 110–114, 1988.
[33]P. Bracconi, L. Nyborg, "Quantitative phase analysis and thickness measurement of surface-oxide layers in metal and alloy powders by the chemical-granular method", Applied Surface Science 133 (1998)129-147.
[34]N. Ordas et al., "X-ray adsoption spectrospy (XAS) and TEM to analyze the precipitation of nanometric oxides of ODS FS obtained by the STARS route. (manuscript under preparation).
[35]M. S. Farkas and A. A. Bauer, "The Solid Solubility and the Constitution of Y in Fe-20 to 40 mass% Cr Alloys," *U.S. Atomic Energy Comm. Publ., BMI-1386*, vol. 20, pp. 1–20, 1959.
[36]E.-S. Lee and S. Ahn, "Solidification progress and heat transfer analysis of gas-atomized alloy droplets during spray forming", Acta Metallurgica and Materialia, vol. 42, no 9 (1994), pp. 3231-3243.
[37]M. Behúlová, J. Mesárošová and P. Grgač, "Analysis of the influence of the gas velocity, particle size and nucleation temperature on the thermal history and microstructure development in the tool steel during atomization", Journal of Alloys and Compound 615 (2014), S217-S223.
[38]G. Hultquist and C. Leygraf, "The initiation of selective oxidation of a ferritic stainless steel at low temperatures and oxygen pressures", Corrosion Science, Vol. 22, No. 4 (1982), pp

331-346.